ESA CONTRACT REPORT

Contract Report to the European Space Agency

WP2300 - Hot Spot Analysis

Joaquín Muñoz Sabater,
Patricia de Rosnay,
Lars Isaksen

Technical Note - Phase-II - WP2300
ESA/ESTEC Contract
4000101703/10/NL/FF/fk

European Centre for Medium-Range Weather Forecasts
Europäisches Zentrum für mittelfristige Wettervorhersage
Centre européen pour les prévisions météorologiques à moyen terme

ECMWF

Series: ECMWF ESA Project Report Series

A full list of ECMWF Publications can be found on our web site under:
http://www.ecmwf.int/publications/

Contact: library@ecmwf.int

European Centre for Medium Range Weather Forecasts
Shinfield Park, Reading, RG2 9AX, England

Contract Report to the European Space Agency

WP2300 - Hot Spot Analysis

Authors: J. Muñoz Sabater,
P. de Rosnay,
L. Isaksen
WP2300 - Hot Spot Analysis
ESA/ESTEC Contract 4000101703/10/NL/FF/fk

European Centre for Medium-Range Weather Forecasts
Shinfield Park, Reading, Berkshire, UK

December 2013

	Name	Company
First version prepared by (December 2013)	J. Muñoz Sabater	ECMWF
Quality Visa	E. Källén	ECMWF
Application Authorized by		ESA/ESTEC

Distribution list:

ESA/ESRIN
Luc Govaert
Susanne Mecklenburg
ESA ESRIN Documentation Desk

SERCO
Raffaele Crapolicchio

ESA/ESTEC
Tania Casal
Matthias Drusch
Klaus Scipal

ECMWF
HR
Division & Section Heads

Contents

Abstract

Contracted by the European Space Agency (ESA), the European Centre for Medium-Range Weather Forecasts (ECMWF) is involved in a global study of monitoring and data assimilation of the Soil Moisture and Ocean Salinity (SMOS) mission data. SMOS is one of the Earth Explorer mission of the ESA's Living Planet Programme, and for the first time, a passive microwave 2D-interferometric radiometer using aperture synthesis is used to observe soil moisture over continental surfaces and ocean salinity over oceans. Since SMOS was launched in November 2009, ECMWF has developed a monitoring chain of SMOS brightness temperatures in near real time, and enhanced the ECMWF Simplified Extended Kalman Filter (SEKF) to support the assimilation of SMOS brightness temperatures for the analysis of soil moisture. In this report a study of the areas where the assimilation of SMOS data is most promising, hereafter call "SMOS hot spots", is carried out.
This report is the technical workpackage number 2300, of Phase II of the monitoring and data assimilation study with SMOS data at ECMWF, contract document number 4000101703/10/NL/FF/fk.

1 Introduction

Monitoring addresses mainly differences between the modelled background field and the observation (i.e. biases, drifts, spikes and jumps in a time series), which are caused by errors of different nature. SMOS brightness temperatures and the model equivalent (computed with the Community Microwave Emission Modeling (CMEM, [6, 3, 14]) platform and described in MS1TN-P1 [4]), are monitored at the European Centre for Medium-Range Weather Forecasts (ECMWF), in Near Real Time (see monitoring reports at [12, 9, 13]). This is a crucial step before assimilating the data. It is expected that the assimilation of SMOS brightness temperatures will be more effective in areas and periods where both the observations and the model background show strong natural variability. These areas and periods are characterized by a high dynamic range in the observed brightness temperatures and sparse to moderate vegetation cover, indicating a high sensitivity to soil moisture and lower effect of the vegetation, respectively. In this report, the monthly and seasonal maps of SMOS hot spots are investigated and constrated with those found by [8].

2 SMOS hot-spots

2.1 Soil moisture - Precipitation feedback

In recent years many studies have demonstrated the crucial role of surface variables, and in particular of soil moisture, for the accurate forecast of atmospheric variables such as precipitation. As part of the Global Land Atmosphere Coupling Experiment (GLACE, [16]), [8] presented several locations of land masses where soil moisture anomalies have an impact on precipitation (see Fig. 1). The model dependence of the results was removed by using an ensemble of global circulation models. They showed that these areas are located mostly in transition zones, where there is enough evaporation to trigger convection and the evaporation fluxes are still sensitive to soil moisture. The study was produced for boreal summers, because in summer evaporation rates are higher and because most of land masses are in the North Hemisphere.

As stated in the introduction, in this study we intend to find areas where SMOS brightness temperatures show a good dynamical range, showing strong sensitivity to variations of soil moisture, as potentially they could be candidates to provide strong feedback to precipitation. In section 2.2, the variability of SMOS observations at monthly scale is investigated. It is also studied the seasonal scale, with particular emphasis in summer of the North Hemisphere, as our results can be directly contrasted to Fig. 1. Complementary, section 2.3 investigates

the variability of the model background to a small positive perturbation of soil moisture.

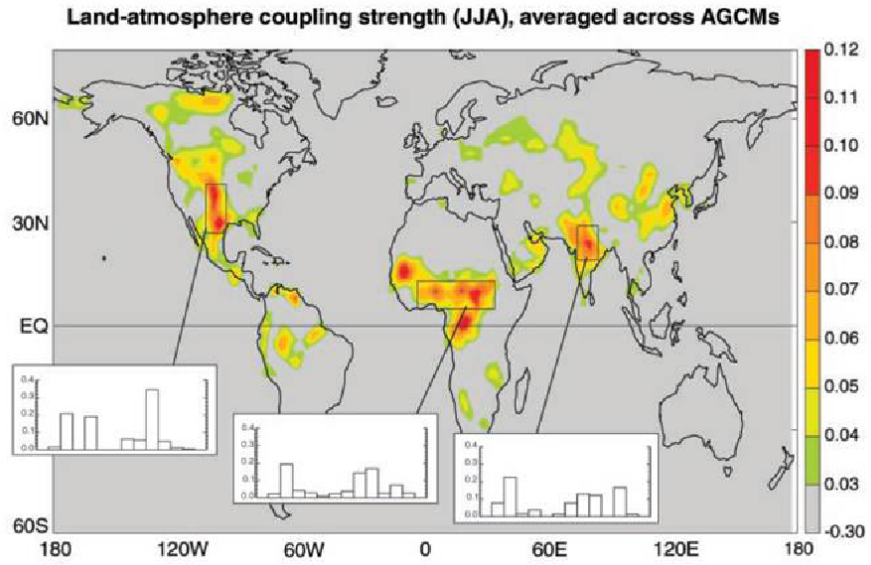

Figure 1: Land-atmosphere coupling strenght for North Hemisphere summer, described as the impact of soil moisture on precipitation. Source:[16]

2.2 Analysis of the SMOS brightness temperatures variability

As reported and shown in [9, 13], maps of the observed brightness temperatures standard deviation provide a good indication of the areas with the strongest variability of the observations. In this report, observed multi-angular and multi-polarised SMOS brightness temperatures from the first reprocessing campaign were used and processed. The period of this study spanned from June 2010 to May 2011. The observations in this period were quality controlled according to:

1. The pure radiometric accuracy of each observation has to be comprised between 0 and 4 K, corresponding to param 012167 of the Near Real Time (NRT) BUFR specification message,

2. Wetlands are avoided by discarding observations with a water content larger than 5%. They correspond to param 013048 of the NRT BUFR specification message,

3. Also, only the alias-free field of view is used to improve the quality of the observations. This information can be found on the bit-5 of the smos information flag, corresponding to the parameter 025174 of the NRT BUFR specification message,

4. Only observations with brightness temperatures between 150 and 330 K are accepted, thus becoming a RFI hard filter,

5. The snapshot quality flag has also been used, corresponding to the parameter 033028 of the NRT BUFR specification message. Only snapshots indicating a 'nominal' quality value were used,

6. Complementary to the previous RFI information, the RFI flag included in the reprocessed product of this study is used as well. It corresponds to the first-bit of the SMOS information flag, BUFR param 025174.

Following the recommendations of [11], SMOS observed brightness temperatures were also averaged in bins of 2 degrees, centered at 40 degrees incidence angle. The resolution chosen for this study was approximately 40 km. Figs. 2a and b show the monthly average of the observations standard deviation for the month of November 2010, using previous filtering steps 1, 2, 3, 4 and 2-degrees binning, for XX and YY polarisation, respectively. They show that the largest variability of the observations occurs in Asia, however this is due to RFI sources contaminating the SMOS signal. We tried to eliminate as much as possible the influence of RFI or corrupted snapshots by using the snapshot quality flag (filtering step 5, Figs. 2c and d). Finally, the RFI information flag, included in the reprocessed product, was also used in this study and the maximum value allowed of monthly standard deviation of brightness temperatures was set up to 50 K, as larger values are not realistic at monthly scale, even at seasonal scales (filtering step 6, Figs. 2e and f). In this way, the RFI influence in these plots is reduced at the cost of having large gaps over Asia, however it does not get rid of all the RFI contamination.

2.2.1 Monthly scale

Fig 3 shows the monthly mean standard deviation of the filtered SMOS brightness temperatures, from June 2010 to May 2011. Fig 4 presents the same information for the YY polarisation. The maximum standard deviation (STD) value allowed was 50 K, as described above. These figures show some regions where the dynamic range of brightness temperatures is high for most of the studied months and both polarisations: Great Plains of the US, Sahel and Argentinian Pampa. Other areas show a strong marked seasonality, as it can be observed at different regions of Australia, in South of Africa and in Western US. It is interesting to observe the strong variability captured in June in the North of India, which is also a potential interesting area. Although this spot is captured for both polarisations, it is within a region influenced by RFI, and therefore it needs of further data to confirm this spot. Europe also presents, together with the remaining of Asia, very strong variability of the brightness temperatures. However, these regions are largely influenced by RFI and although potentially interesting since the meteorological point of view, these plots are not sufficient to identify hot-spots areas.
At the end of December 2010, a stability test of the SMOS platform took place during 6 days, no data was produced during this period. During the following 2 weeks the science data was degraded and, in addition, the NRT processor did not work nominally until 18 February 2011, as during all this period the observed brightness temperatures were a few degrees larger, producing larger bias. This had an effect also in the reprocessed product used in this study, and this is why January-2011 presents no data in both Fig 3 and 4, and February larger gaps. The conclusions for the YY polarisation are quite similar, although a slightly lower monthly dynamical range can be observed because this polarisation is less sensitive to variations of soil moisture than XX polarisation.

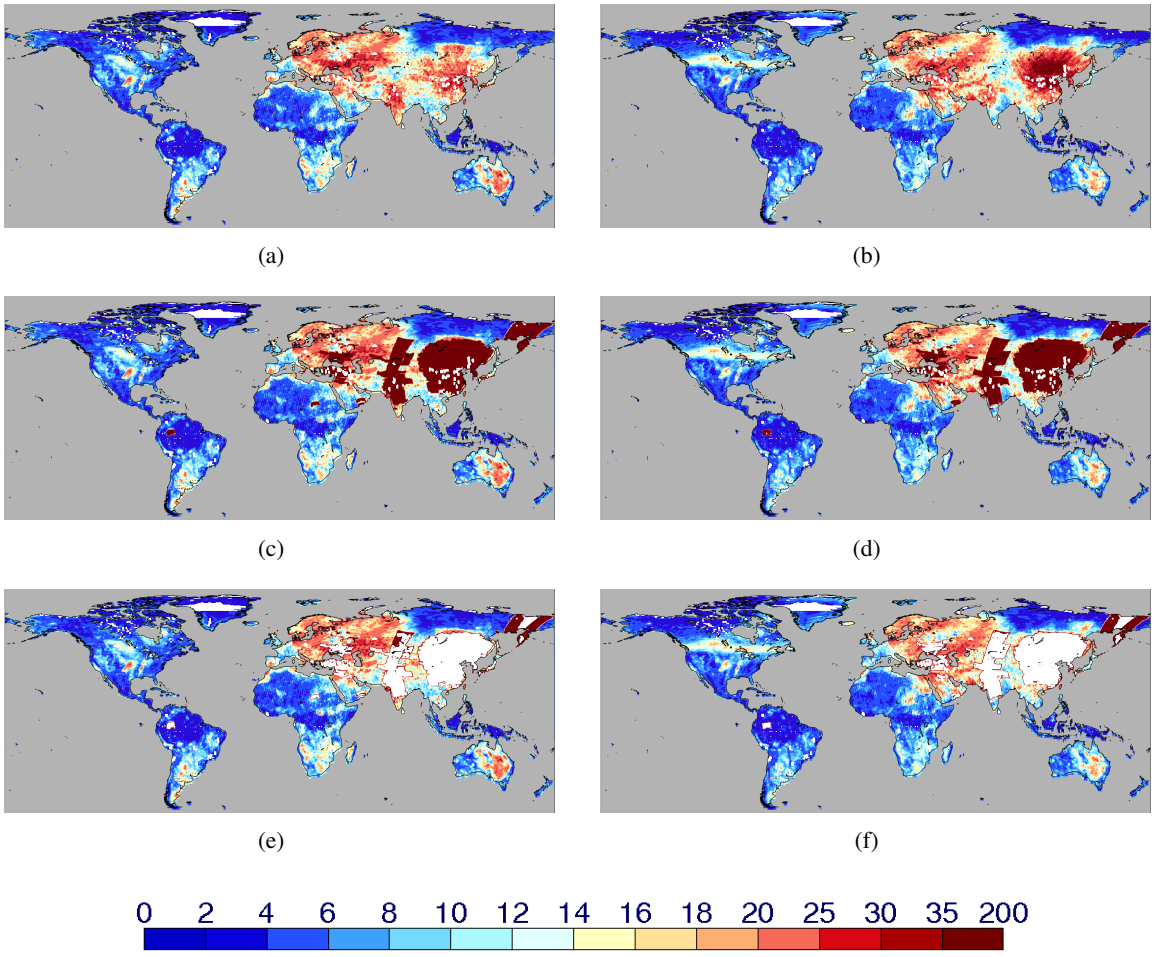

Figure 2: Averaged standard deviation (STD) of the SMOS observed brightness temperatures (in K) for November-2010. Left column is for XX polarisation and right column for YY polarisation; a) and b), using filtering steps 1, 2, 3, 4 of section 2.2 and 2-degrees binning ; c) and d) adding also the snapshot quality information flag; e) and f) adding the RFI information flag and limiting the maximum value allowed of brightness temperatures STD to 50 K.

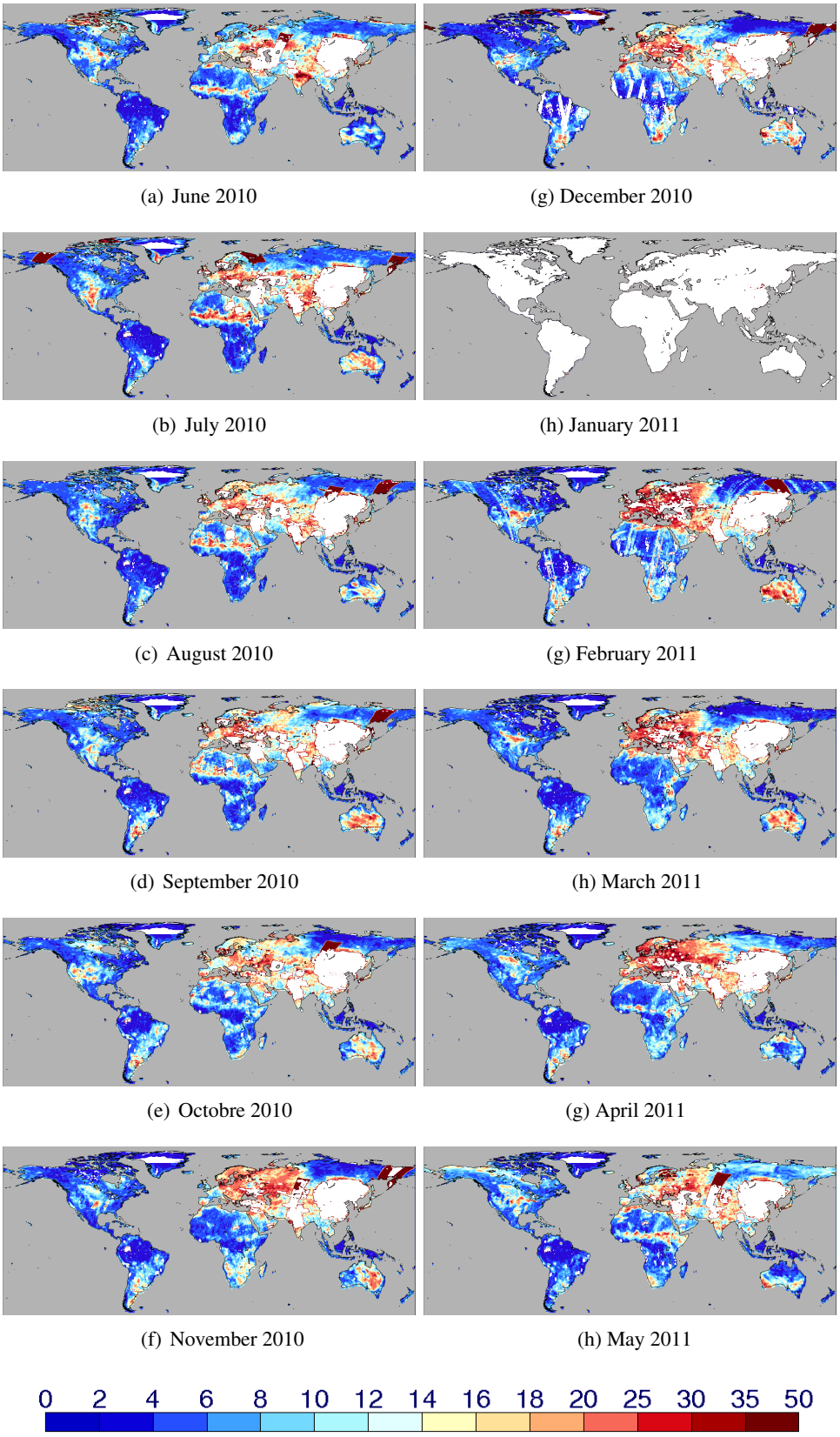

Figure 3: Monthly averaged SMOS brightness temperatures (in K), for XX polarisation. Observations were filtered according to section 2.2.

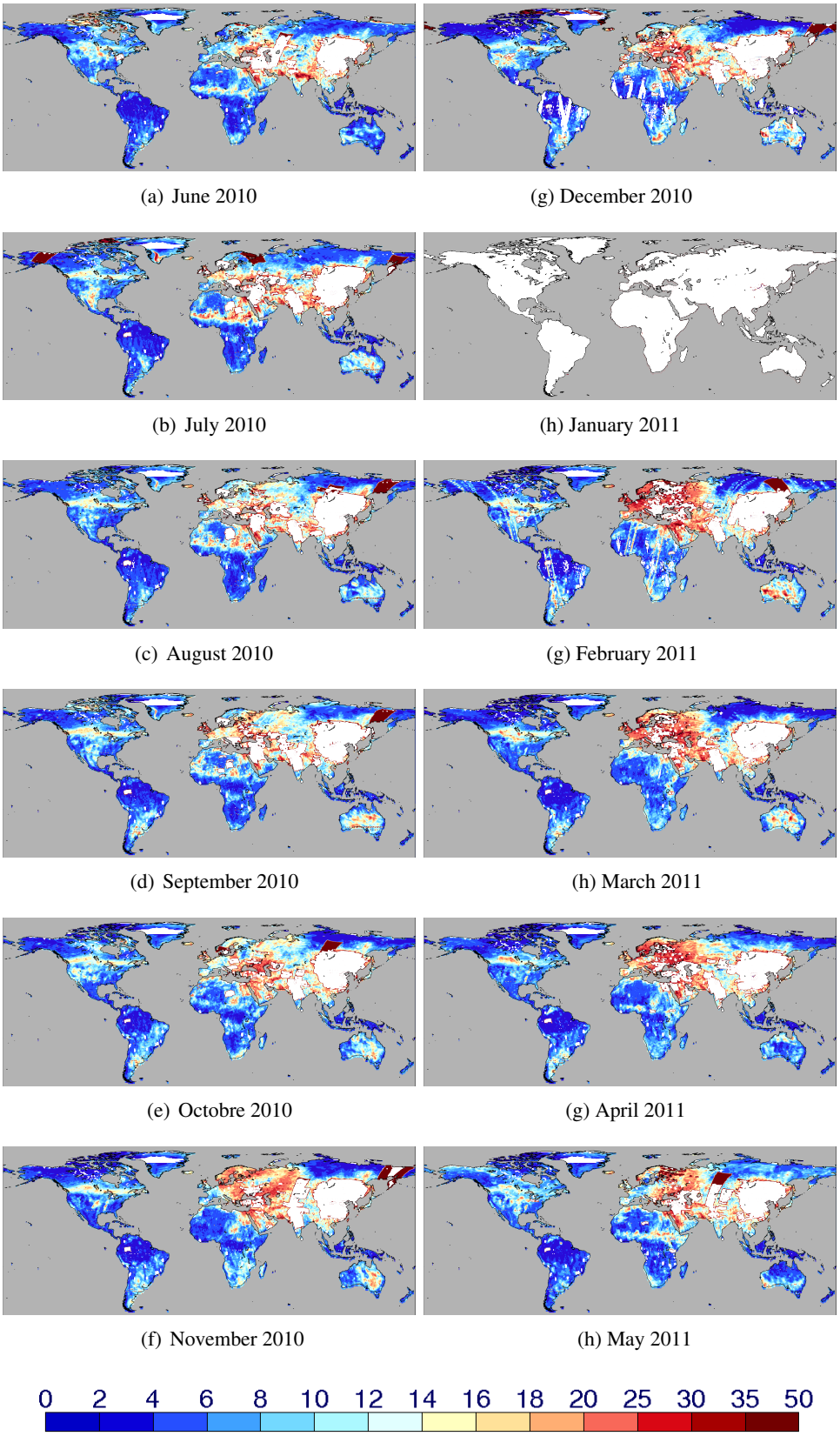

Figure 4: As Fig.3 but for YY polarisation.

2.2.2 *Seasonal scale*

The two plots of Figs. 5 show the average standard deviation of SMOS brightness temperatures for the boreal summer of 2010, as it was done in [16], applying all observation filters of section 2.2, for XX and YY polarisation, respectively. Compared to Fig. 1, it can be observed that the Great Plains of USA, the Sahel, the land mass at the East of Africa facing the Mozambique Channel, the far North of Canada and North of Mexico, have them all a broad range of SMOS brightness temperatures. Consequently, in these areas, SMOS could provide very valuable information about the water content of the soil, which could be used, among others, in data assimilation systems with the objective of improving the predictability of atmospheric variables, such as precipitation or air temperature.
In contrast to the hot-spot observed in the Amazon in Fig. 1, the SMOS signal has a very low variability in this area. Also, the hot-spots predicted in Asia are hidden by RFI in the SMOS signal and no conclusions can be extracted for this large region without more recent data, which partly, removes the RFI influence. The dynamic range of SMOS brightness temperatures is also very large in Australia, but according to Fig. 1, this is not a hot-spot region, at least for boreal summers, i.e., the variability of soil moisture has not got a significant feedback in to precipitation.

Figs. 6 and Fig. 13 show similar plots as Figs. 5 and 12, but averaging is now done for summer of the South Hemisphere, covering the months of December, January and February. This season was not explored in the study of [8], and could also be interesting due to stronger evaporation rates in the South Hemisphere. The quality of Fig. 6 is, however, hampered by the degraded data of this period. With the available data, these figures still show both, good amplitude of seasonal brightness temperatures and good sensitivity of the model to perturbations of soil moisture, in the Center of US, the Argentinian Pampa, the South of Africa and Australia. These regions are potential hot-spots for austral summers, but they need to be confirmed through experimentation which will investigate the impact of assimilating SMOS data in the forecast of atmospheric variables.

Finally, spring and autumn seasons were also studied (see Appendix-A). As a new feature, the observations show large variability in Canada and also in the North of Asia, likely due to the snow melting and beginning of the snow season. Sahel, South of Africa and Australia show also good variability of the observed brightness temperatures and good sensitivity of the model for both, spring and autumn seasons.

In tables 1 and 2 two domains covering, approximately, the Central US and Sahel were chosen in order to compute the averaged seasonal values of the SMOS brightness temperatures STD (left panel). These two regions have the strongest response to variations of soil moisture. Apparently, winter months (Dec., Jan., Feb.) obtain the highest STD for Central US, but this value is artificially increased by some RFI contamination. Summer shows the strongest response, 15.7 K, which is well over the whole America average of 8.7 K for these months, being July the most responsive month (Fig. 3). The spring season of 2011 also shows good sensitivity in Figs 3 and 14, but the sensitive area is located more towards the North of the region covered in Table 1, due to the soil water variations produced by snow melting. The situation for the YY polarisation is similar, but this polarisation is less sensitive to variations of soil moisture than XX polarisation, and the STD values are lower, but still significantly higher than the mean averaged of America for YY polarisation, which is 8.6 K.
The left panel of table 2 represents the same values that the above, but for the Sahel region. During the whole period of study this area was very little influenced by RFI. The summer season presents a strong averaged value of STD, for both polarisations, which is very superior to the mean value for all Africa (11.1 K for XX polarisation and 10.1 K for YY polarisation). This is somehow expected as during these months that the West African monsoon occurs. Autumn also presents good sensitivity to soil moisture variations, whereas the lowest values are obtained for the winter season, lower than 10 K in average.

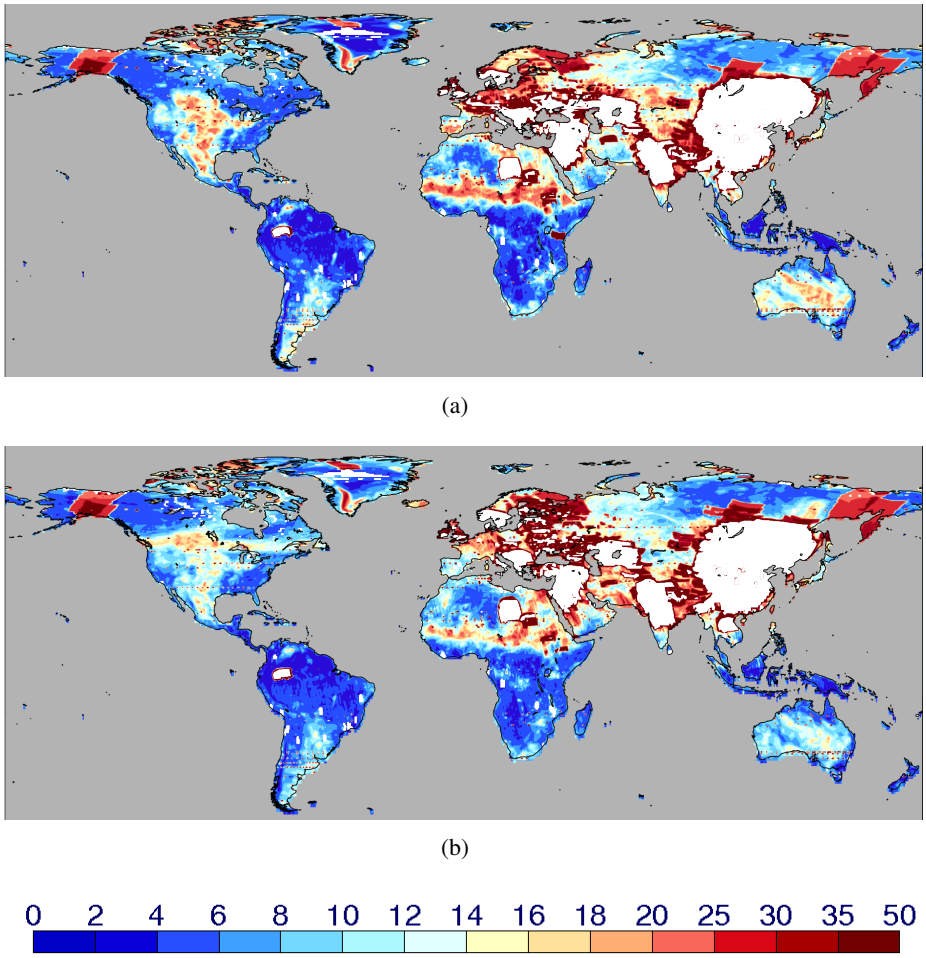

Figure 5: Averaged standard deviation of the SMOS observed brightness temperatures (in K) for June, July and August 2010. Top plot is for XX polarisation and bottom plot is for YY polarisation; observations were filtered as described in section 2.2.

	STD		Jacobian	
	XX	**YY**	**H**	**V**
J-J-A	15.7	12.3	-118.5	-89.9
S-O-N	12.9	10.6	-121.7	-92.4
D-J-F	17.1	12.7	-79.2	-58.9
M-A-M	11.7	9.5	-87.1	-62.6

Table 1: Averaged seasonal standard deviation of SMOS brightness temperatures (in K), for the Center of US and North of Mexico, for XX and YY polarisation (left panel). Observations were filtered according to section 2.2. Right panel shows the averaged seasonal first SMOS component of the model Jacobians (in K/m^3m^{-3}) at 40 degrees incidence angle (see section 2.3). The latitude/longitude limits of the domain accounted for were: lat: 28 N, 46 N ; lon: 108 W, 98 W. J-J-A=June, July, August, S-O-N=September, October, November, D-J-F=December, January, February, M-A-M=March, April, May.

	STD		Jacobian	
	XX	**YY**	**H**	**V**
J-J-A	19.3	16.2	-92.0	-62.0
S-O-N	14.7	12.7	-116	-80.5
D-J-F	8.1	7.2	-115.8	-79.4
M-A-M	9.0	8.5	-45.8	-10.9

Table 2: As Table 1 but for the Sahel region. The latitude/longitude limits of the domain accounted for were: lat:9.2N, 18.5N; lon: 15.1W 36.6E

.

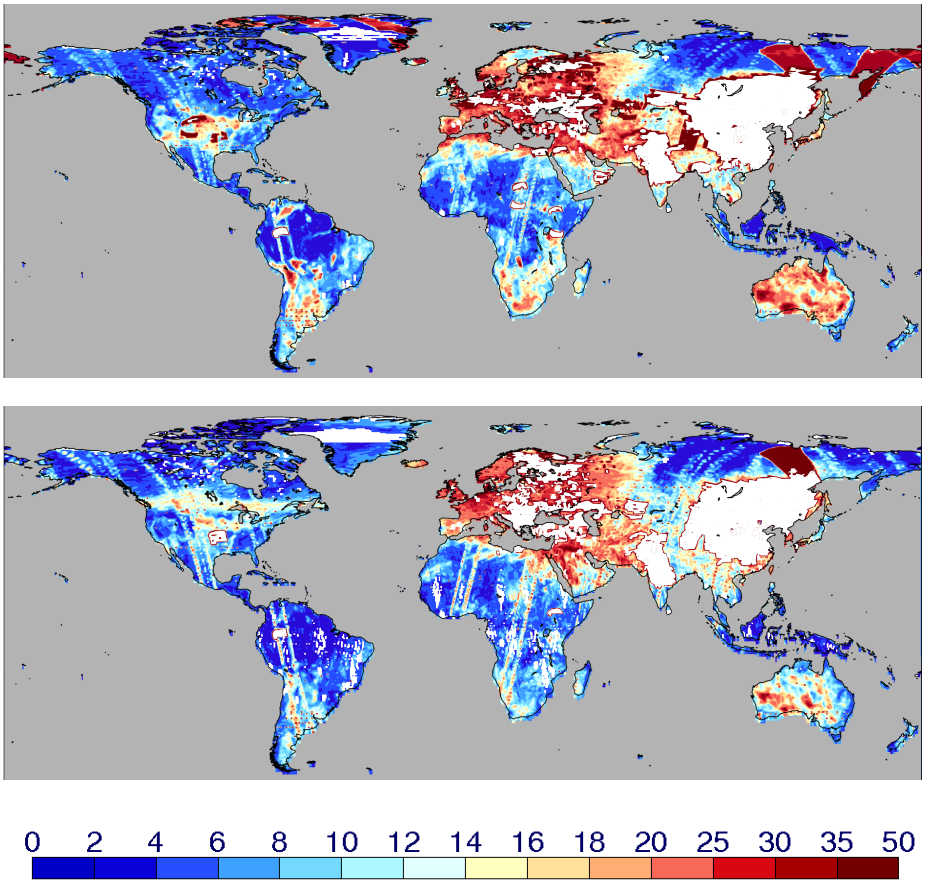

Figure 6: As Fig. 5 but average is done for December 2010, January and February 2011.

2.3 Analysis of the model variability.

In this section the sensitivity of the simulated brightness temperatures to variations of soil moisture is investigated. To be consistent with section2.2, both, the monthly and seasonal scales were studied. A soil moisture perturbation of $\delta\theta$ of $0.01 m^3 m^{-3}$ is applied to the soil first 7 cm, because it was found it was the best value This corresponds to study the first component (for a given angle α and polarisation p) of the SMOS Jacobian matrix;

$$J^{SMOS}_{(0-7cm)}(\alpha, p) = \frac{T'_B(\alpha, p) - T_B(\alpha, p)}{\delta\theta} \quad (1)$$

with $T'_B(\alpha, p)$ being the simulated brightness temperatures when the soil moisture θ was increased by $\theta = \theta_0 + 0.01 m^3 m^{-3}$, in respect to the simulated value $T_B(\alpha, p)$ with $\theta = \theta_0$. This is the component of the SMOS Jacobian showing larger sensitivity to soil moisture perturbations, mainly because the emissivity of the soil components have a large dependency on the soil water content of the first few cm. of soil

A new suite was developed to run two one-year simulations of the ECMWF L-band radiative transfer model CMEM, one to compute $T_B(\alpha, p)$ and the other for $T'_B(\alpha, p)$. Simulations were carried out at T255 spectral resolution, from June 2010 to May 2011. The parameterisations used for the main components influencing model brightness temperatures were the Wang and Schmugge, 1980 [18] dielectric model, the Wigneron et al., 2001 [20] for the soil roughness and the Wigneron et al., 2007 [19] for the vegetation emissivity. The combination of these parameterisations, together with the Wigneron et al., 2001 [20] model of the effective temperature and the Pellarin et al., 2003 [15] for the atmospheric contribution, has shown to be the most consistent at global scale with the reprocessed observations of SMOS brightness temperatures used in this study, in terms of lower bias and higher correlation values [5]. The simulations were forced with operational analysed fields and regridded to the ECMWF T255 reduced Gaussian grid (equivalent to an approximately 80 km horizontal resolution). Seasonality in the vegetation was allowed, by using a LAI monthly climatology based on a MODIS satellite product [2]. Vegetation cover fraction and type from HTESSEL [1] were also used in these simulations. Finally, soil texture data is obtained from the Food and Agriculture Organization (FAO) data set, whereas sand and clay fractions have been computed from a lookup table according to [17]. Simulations were run only at $\alpha = 40$ degrees incidence angle and horizontal (H) and (V) polarisations.

2.3.1 Monthly scale

Figs. 7 and 9 show the monthly averaged sensitivity of simulated brightness temperatures to a perturbation of the first 7 cm of soil of $0.01 m^3 m^{-3}$, at 00UTC and for H and V polarisations, respectively. Figs. 8 and 10 are the equivalent figures at 12UTC. This separation between 00UTC and 12UTC was done in order to study also the influence of the daily cycle of soil moisture in the averaged monthly sensitivity of brightness temperatures. These figures show a quite strong seasonality of the model sensitivity to variations of soil moisture, being the summer months of the North Hemisphere those showing stronger sensitivity in general, whereas it is also stronger in the H polarisation than in the V polarisation. The North of Africa shows the largest sensitivity and a very strong annual range of jacobian values, being greater than $500\ K/(m^3 m^{-3})$. At this zone, large sensitivity is obtained, lower than $-250\ K/(m^3 m^{-3})$ at 00UTC during winter months of North Hemisphere, whereas it can reach values larger than $250\ K/(m^3 m^{-3})$ in spring and summer months of North Hemisphere. This is one of the few regions showing a "positive" sensitivity, i.e., an increment of brightness temperatures produced by an increase of soil moisture. The reason for this is the following:
Fig. 11 shows the effective temperature difference when a $0.01 m^3 m^{-3}$ of water was added to the first 7 cm of

soil, averaged for June 2010. It shows that over desertic and very dry areas of North of Africa and Middle East, the effective temperature increases significantly with increasing soil moisture. When soil moisture increases then the effective temperature sampling depth decreases too, and therefore the effective temperature gets closer to that of the surface. Since for desertic areas the surface temperature is higher than the deep soil temperature (due to the strong radiative heating in desertic areas), then the effective temperature increases too with increasing soil moisture.
Another way to understand this effect is by looking at the model of the effective soil temperature used in this study, which is that of Wigneron et al., 2001 [20]:

$$T_{eff} = T_{deep} + (T_{surf} - T_{deep}) \times C; \qquad C = (\frac{w_s}{w_0})^b \tag{2}$$

being T_{deep} the deep soil temperature (in this study equivalent to that of the third soil layer of the land surface model (28-100 cm)), T_{surf} the surface temperature (in this study equivalent to the first soil layer (0-7 cm)), and C a variable which is a function of the surface soil moisture (w_s) and two semi-empirical constants w_0 and b. A positive perturbation of surface soil moisture will make the C variable grows, and then the effective temperature will be closer to the surface temperature. The difference between the perturbed and unperturbed runs will be larger as the unperturbed surface soil moisture is drier, and maximum when is zero, i.e., in deserts.
In the Integrated Forecasting System (IFS) version, an increase of soil moisture will also lead to an increase of the evapotranspiration, which makes the effective temperature slightly decrease. This effect is not accounted for in the offline version, being this the main limitation of the offline jacobians computed here. However, the sampling depth effect dominates in desertic areas, and in the IFS version it is also expected that a positive perturbation of soil moisture leads to an increase of brightness temperatures.

In summary, the strongest sensitivity of the model brightness temperatures to soil moisture perturbations were found in the boreal summer of the North Hemisphere, with H polarisation exhibiting a stronger sensitivity than V polarisation. Significant sensitivity was found in the Great Plains and intermountain regions (between Rocky and Pacific coast) of US, in far North of Canada in boreal summers, in Australia (specially Western Australia), Andes and Patagonia, South Africa (Namib and Kalahari deserts), Sahel, North Africa around Sahara desert (with positive sign of the jacobians in spring and summer months), Gobi desert, Arabian Peninsula and Plateau of Iran.

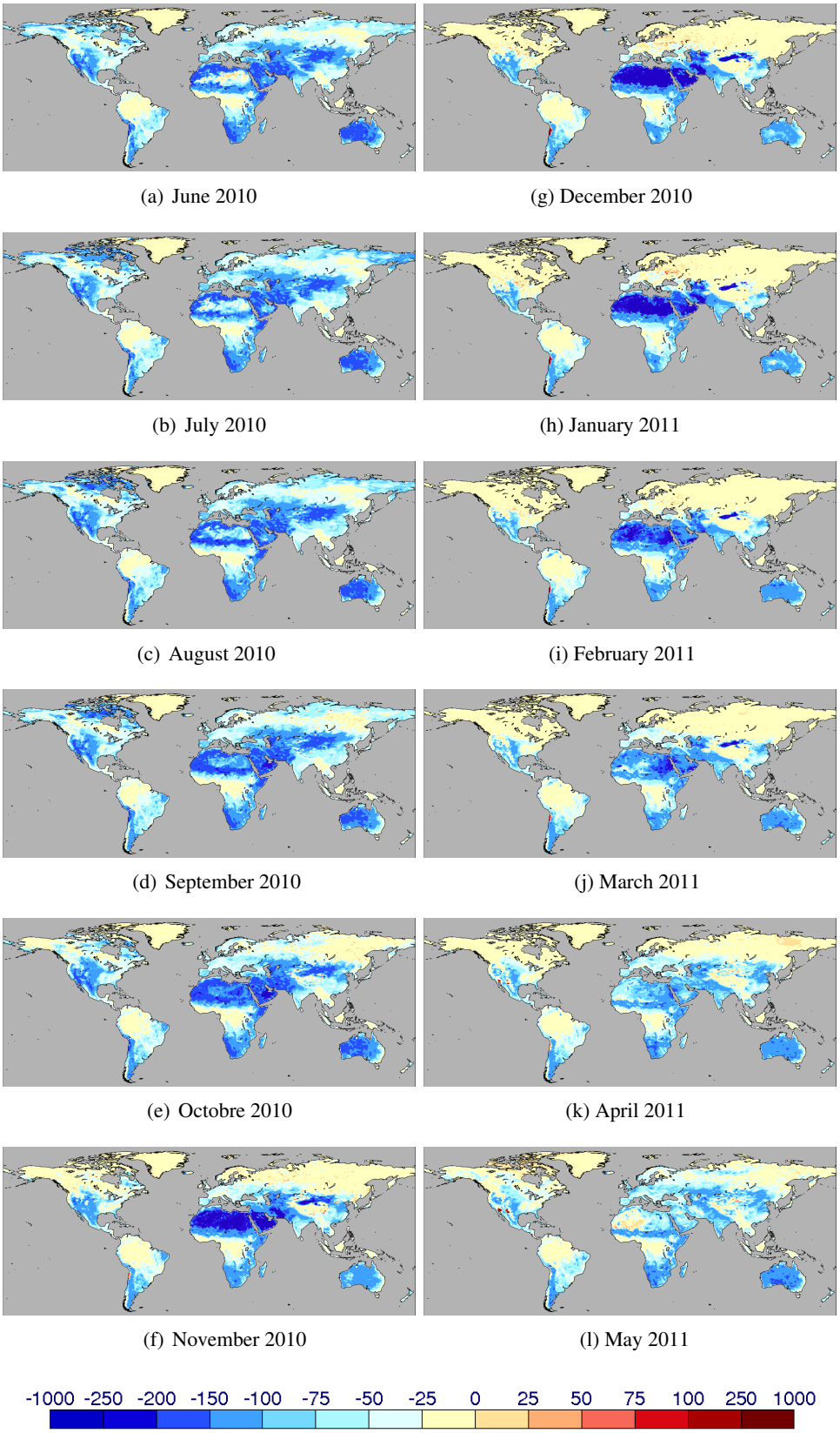

Figure 7: Monthly averaged first component of the SMOS Jacobians in $K/(m^3 m^{-}3)$ (see section 2.3) at 00UTC and H polarisation

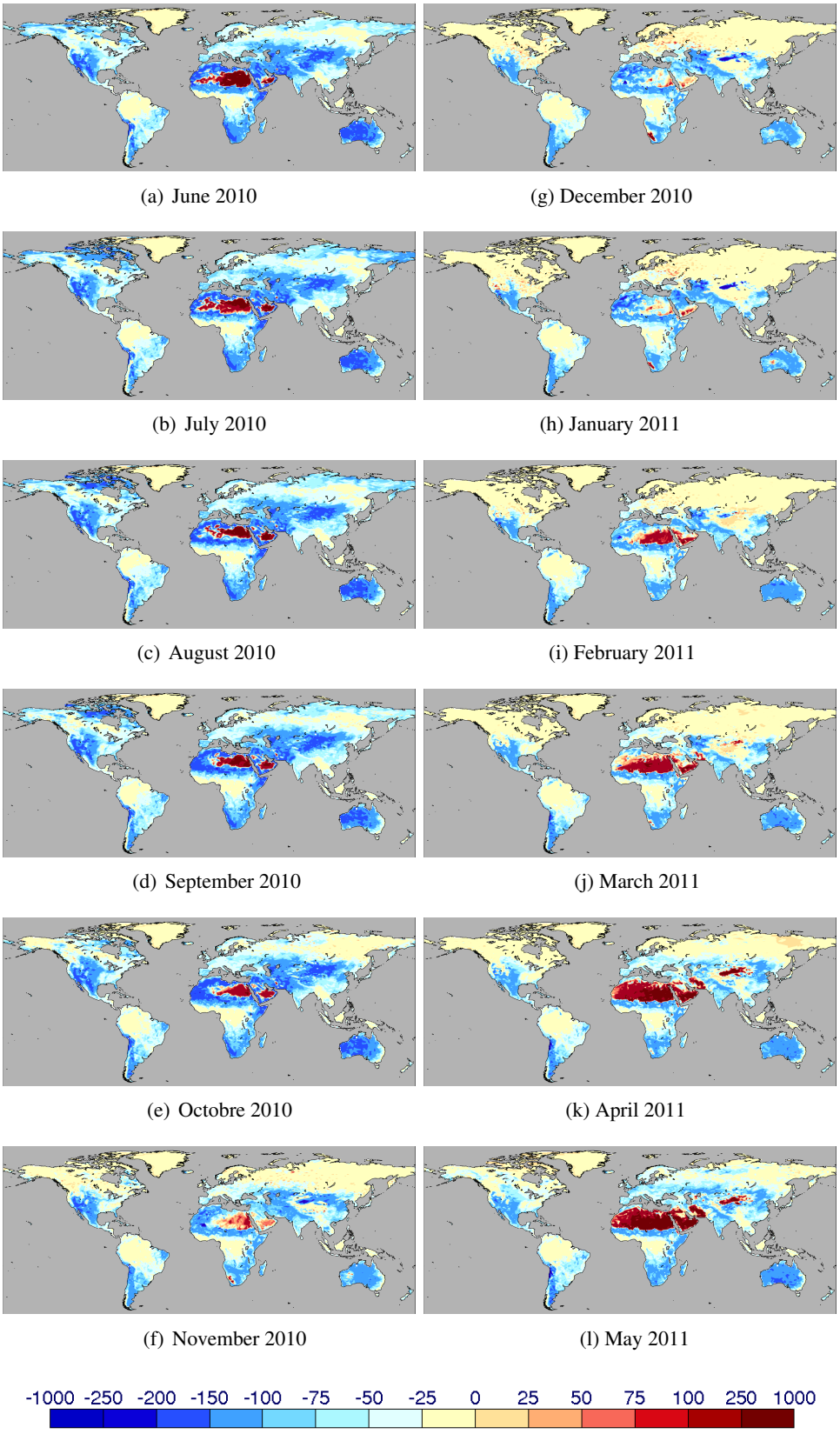

Figure 8: As Fig.7 but at 12UTC.

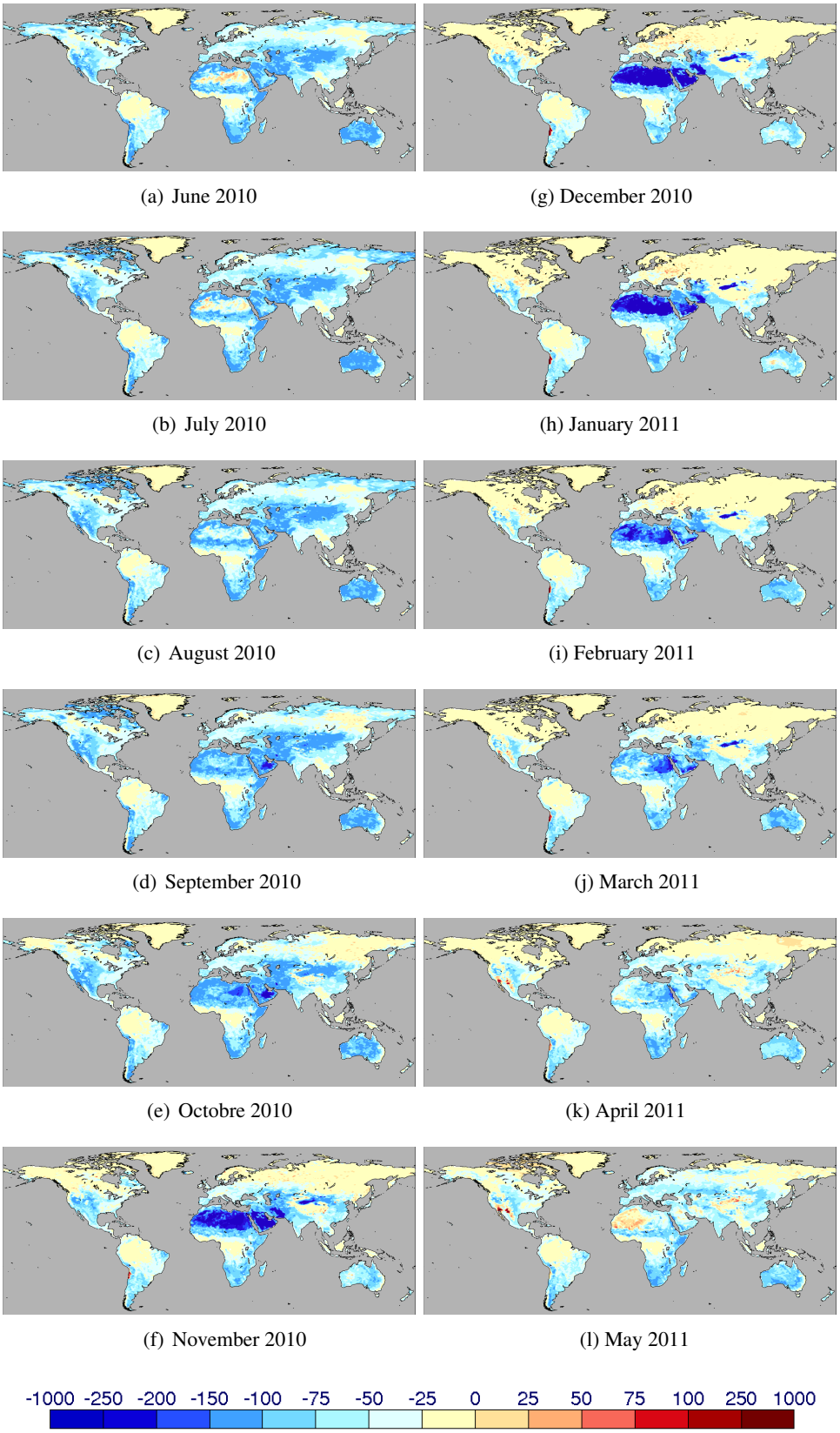

Figure 9: As Fig.7 but for V polarisation.

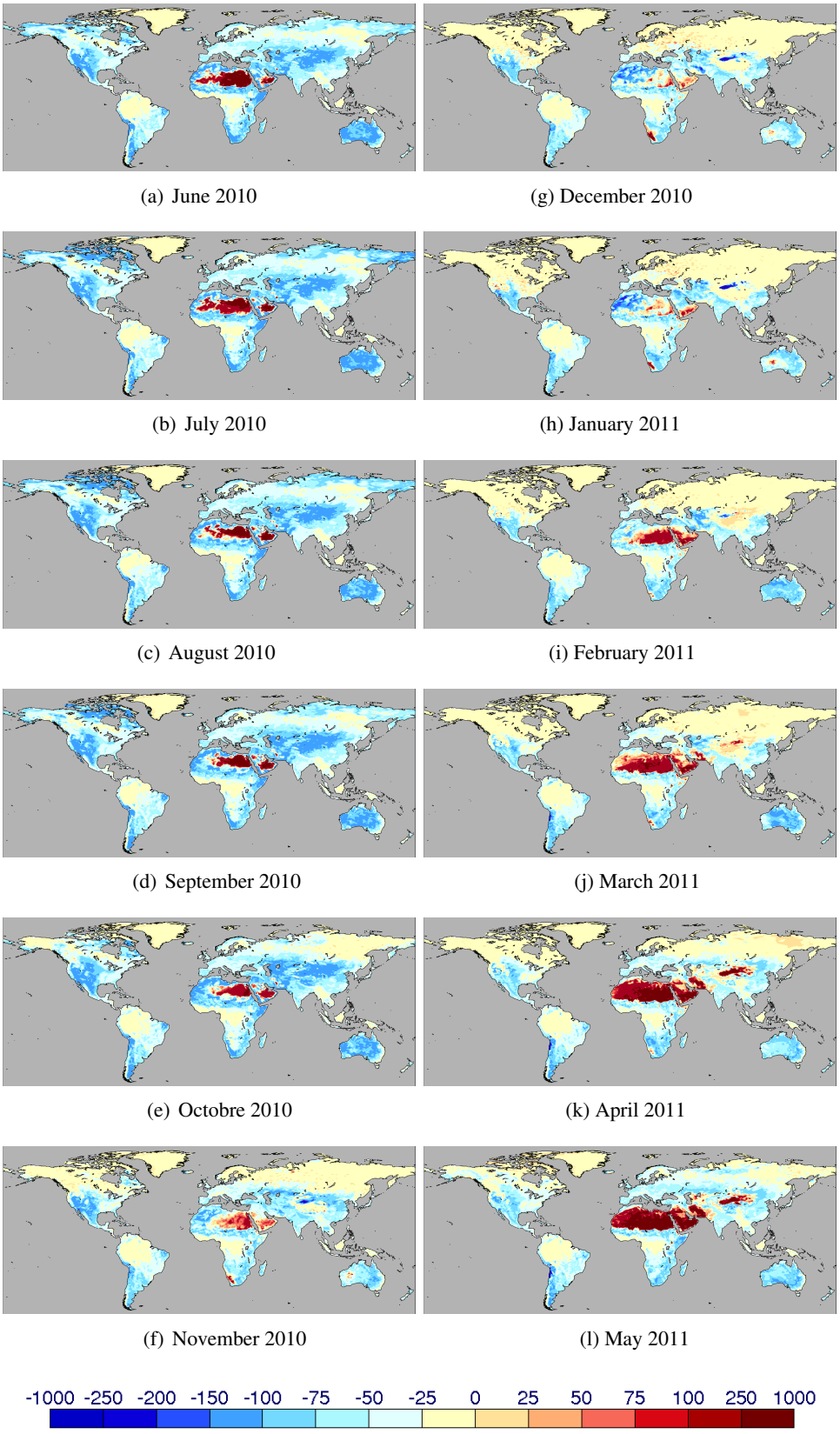

Figure 10: As Fig.7 but at 12UTC and V polarisation.

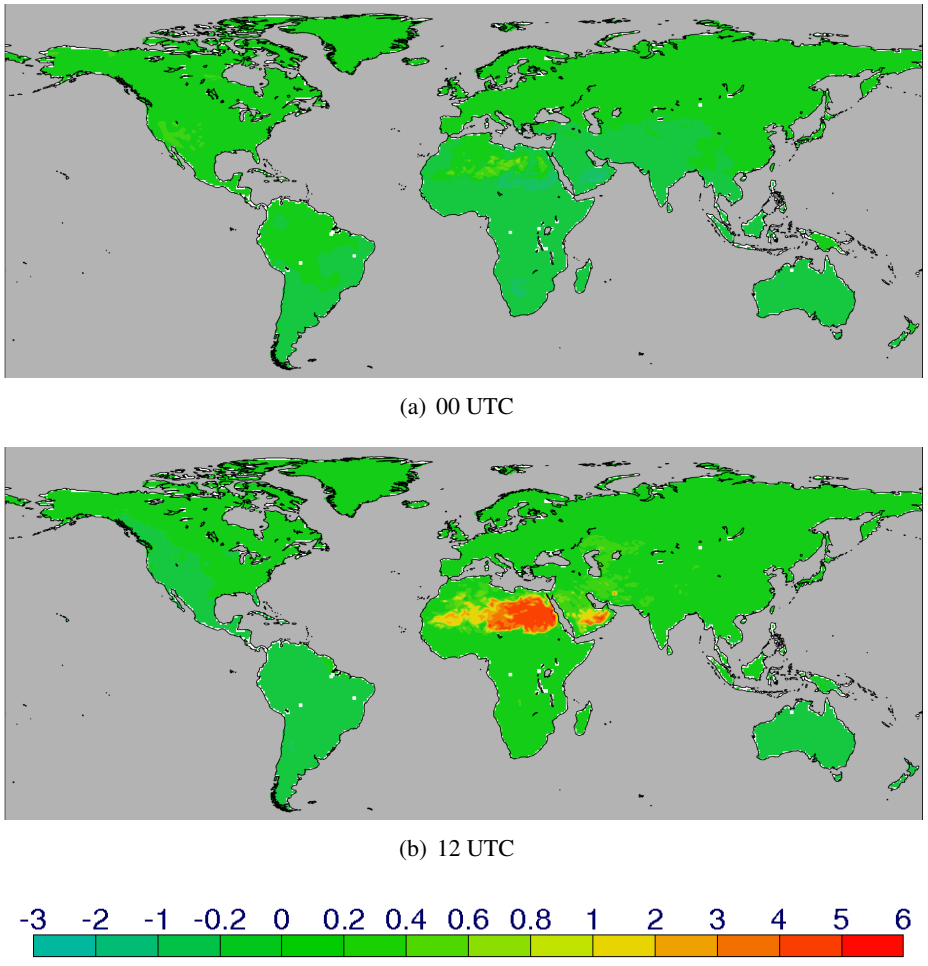

(a) 00 UTC

(b) 12 UTC

Figure 11: Effective temperature difference (in K) obtained when the soil was wettered with an extra $0.01 m^3 m^{-3}$ *compared to its initial value. These figures show mean values for June 2010.*

2.3.2 *Seasonal scale*

Fig. 12 shows the averaged jacobians studied in section 2.3 during boreal summers, for H (left) and V (right) polarisation. The West-Center of the US and the Sahel regions present strong sensitivity of the model brightness temperatures to small perturbations of soil moisture. This is consistent with the large seasonal dynamical range of brightness temperatures, in response to variations of soil moisture, which was found in the previous section. The model is also very sensitive in the far North of Canada, all the North of Africa and Middle East (the lattest are partly due to an artifact of using an uncoupled land surface/radiative transfer system, therefore not accounting for the evaporative cooling, see discussion in section 2.3.1), South of Africa, in particular the Western part, Center of Asia and West-Center of Australia. The sensitivity shown by the model is notably larger for H than for V polarisation, as it could be expected.

The right panel of tables 1 and 2 present averaged values of the Jacobians at 40 degrees incidence angle when a positive perturbation of $0.01 m^3 m^{-3}$ of water was applied to the first 7 cm of soil, for the Central US and the Sahel domains, and for H and V polarisation. In contrast to the observations STD, now winter months obtain the lowest values, below 80 $K/m^3 m^{-3}$, because the effect of RFI does not affect the model. However, the autumn season seems to slightly overestimate the sensitivity to soil moisture perturbations if they are compared to the slightly lower summer values. This strong sensitivity in autumn seems to be caused in September and October rather than in November, when the Jacobian values were much smaller. The trend is the same for both polarisations, but as it could be expected the V polarisation is less responsive than H polarisation, in average it presents 0.2-0.3 K lower response.
For the Sahel domain (table 2), the lowest reactivity is found to be in spring, which is consistent with the lower range of brightness temperatures found in this season. The lowest jacobians values obtained in spring and summer can also partially be explained because the vegetation is more developed, reaching its peak in August. Therefore the effect of the vegetation is larger and the sensitivity to soil moisture decreases. However, the winter months present relatively strong jacobians values compared to the relatively low range of brightness temperatures. Indeed, all values are negative at 00UTC during winter months, whereas some few positive values are obtained at 12UTC, and therefore there is almost no compensation with positive values. In the winter case, the soil surface is colder than in other months and the sampling depth effect is lower (see discussion in 2.3.1).

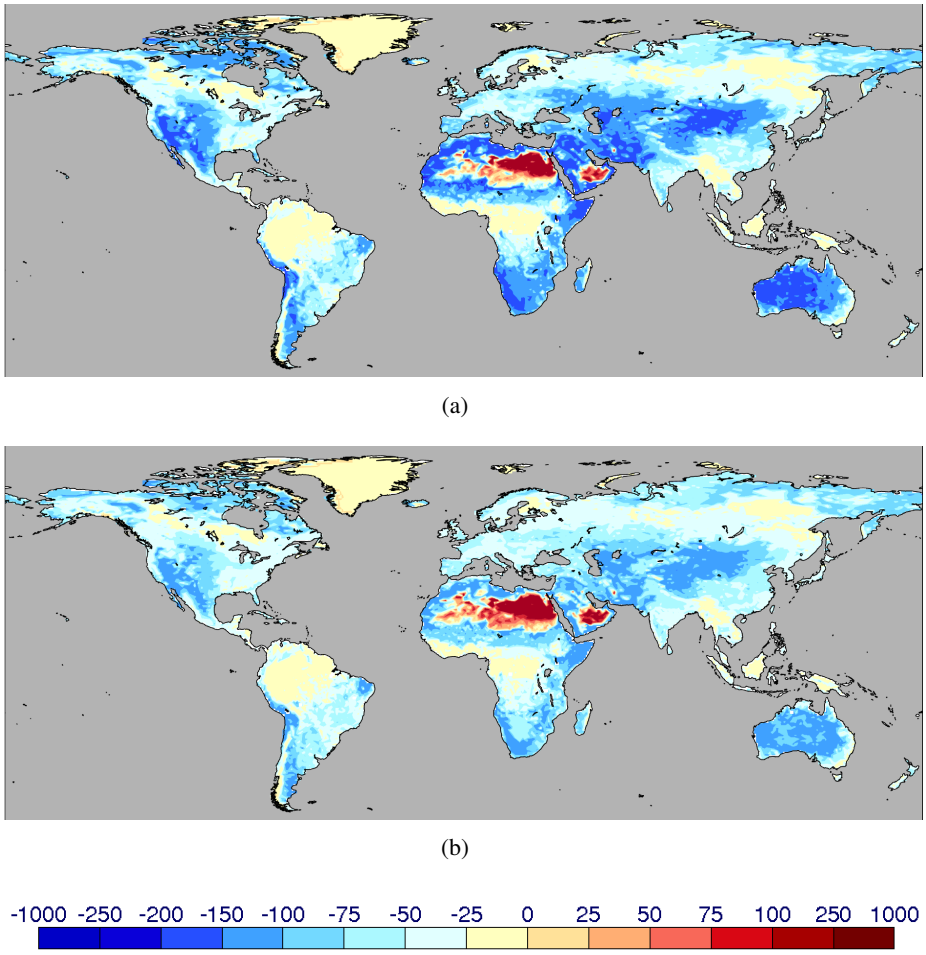

Figure 12: Averaged first component of the SMOS Jacobian (in K/m^3m^{-3})(see section 2.3) for June, July and August 2010. Top plot is for XX polarisation and bottom plot is for YY polarisation.

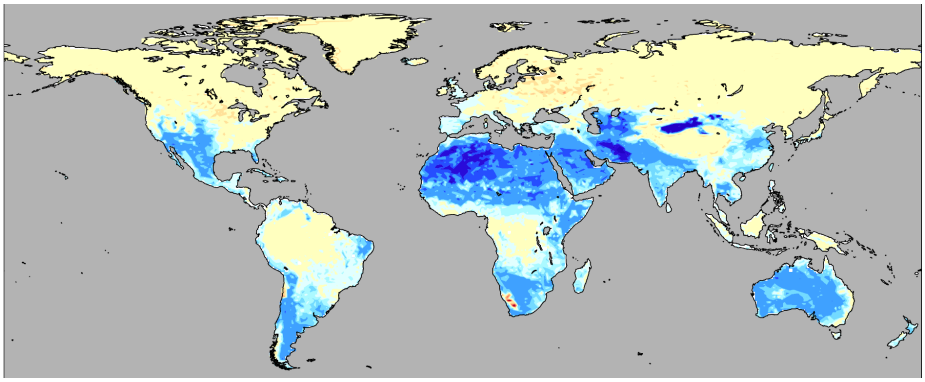

(a)

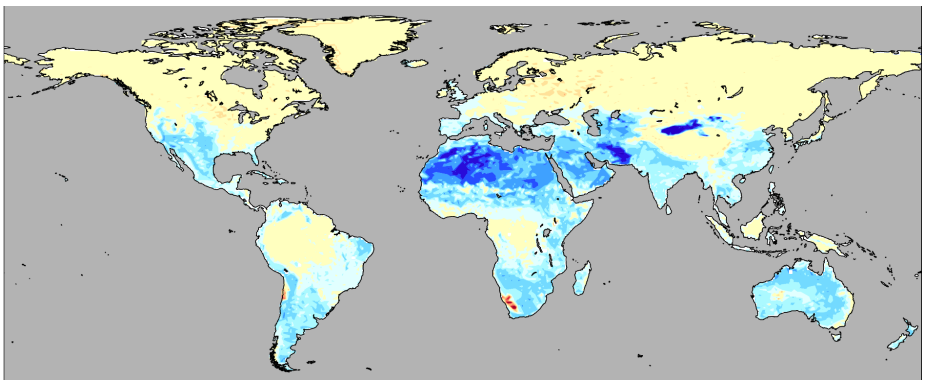

(b)

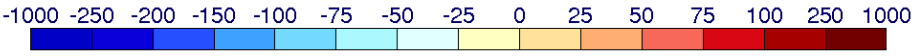

Figure 13: As Fig. 12, but average is done for December 2010, January and February 2011.

3 Conclusions

This work intends to localize areas showing strong sensitivity of SMOS brightness temperatures to soil moisture variations and large sensitivity of the model to small perturbations of soil moisture. They are characterized by a large range of brightness temperatures and low to moderate LAI. It was found that the center of the US and the Sahel regions accomplish the previous requirements, but furthermore they are in the hot-spot areas found by [16]. This means that they are the regions most promising in terms of soil moisture-precipitation feedback and, additionally, their assimilation in the ECMWF SEKF could enhance the accurate initialization of soil moisture and the forecast of near-surface atmospheric variables. However, other regions were shown to be potentialy interesting too, at least for a better access to soil moisture, as South of Africa, North of Canada or Australia.
The results found in this study need to be confirmed with long-term experiments, showing the potential feedback of SMOS hot-spots in the forecast skill of surface and atmospheric variables. Thus, the results obtained here will be cross-correlated with those obtained in reports [10] and [7].

Acknowledgements

This work is funded under the ESA-ESRIN contract number 20244/07/I-LG. Acknowledgements to Matthias Drusch and Susanne Mecklenburg, both ESA staff, for their contribution in the project definition.

4 Appendix-A

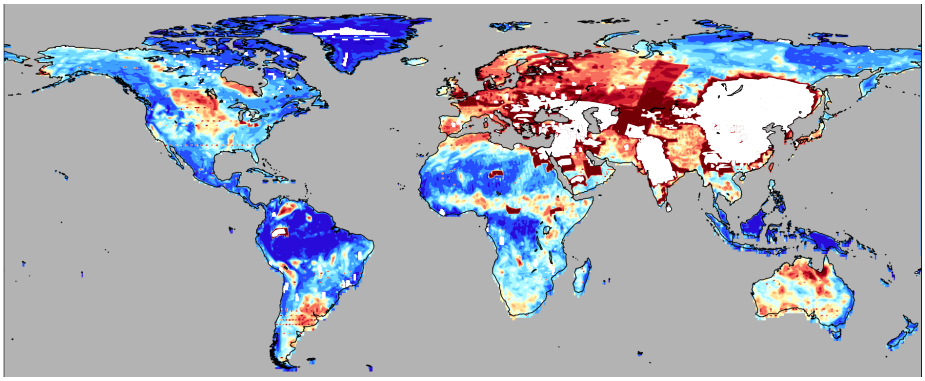

(a) XX polarisation

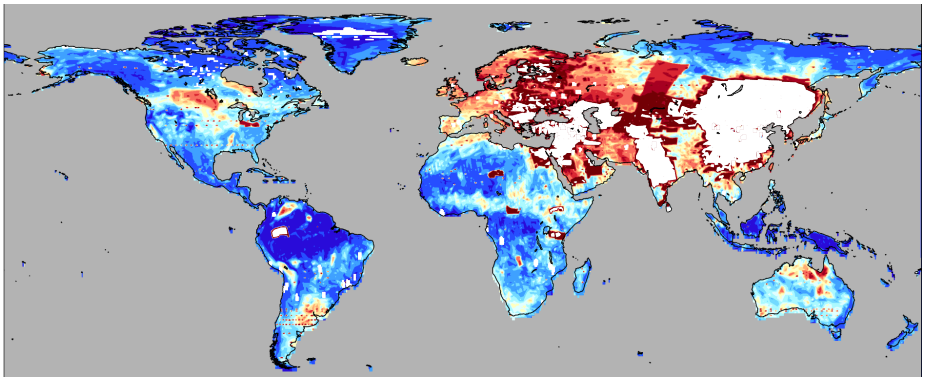

(b) YY polarisation

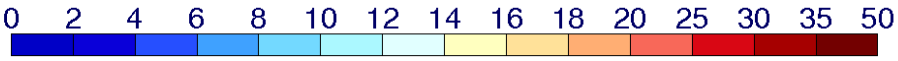

Figure 14: Averaged standard deviation of the SMOS observed brightness temperatures for March, April and May 2011. Top plot is for XX polarisation and bottom plot is for YY polarisation; observations were filtered as described in section 2.2.

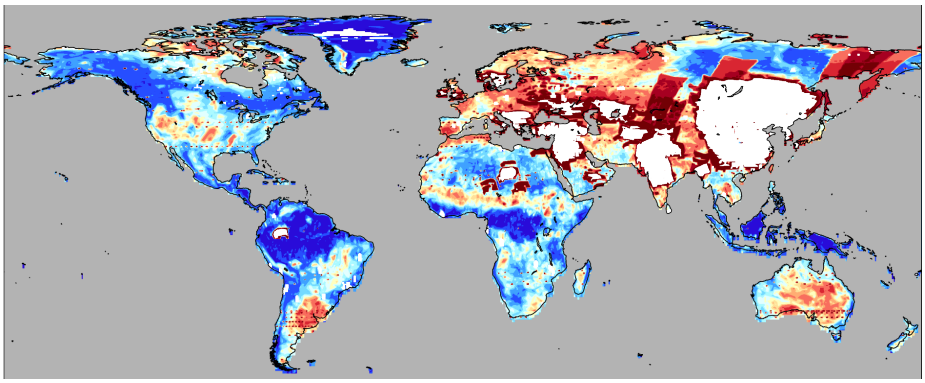

(a) XX polarisation

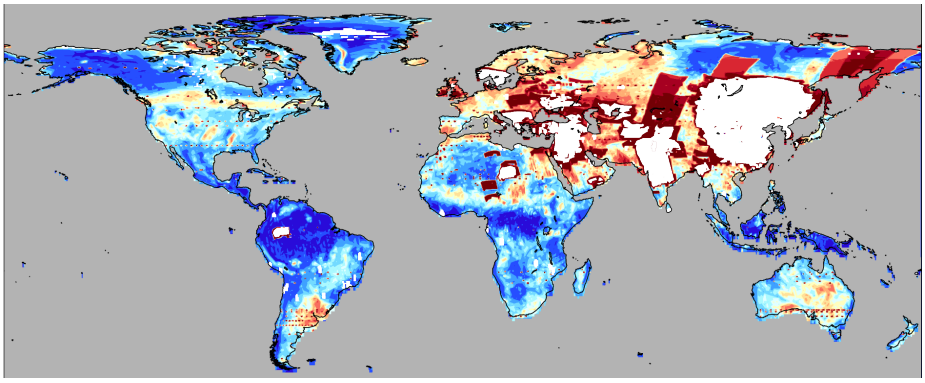

(b) YY polarisation

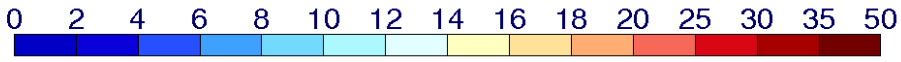

Figure 15: As Fig. 14, but average is over September, October and November 2010.

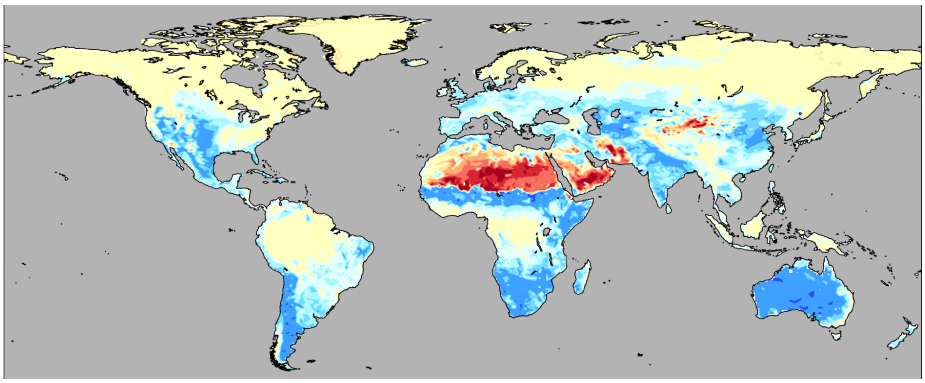

(a) H polarisation

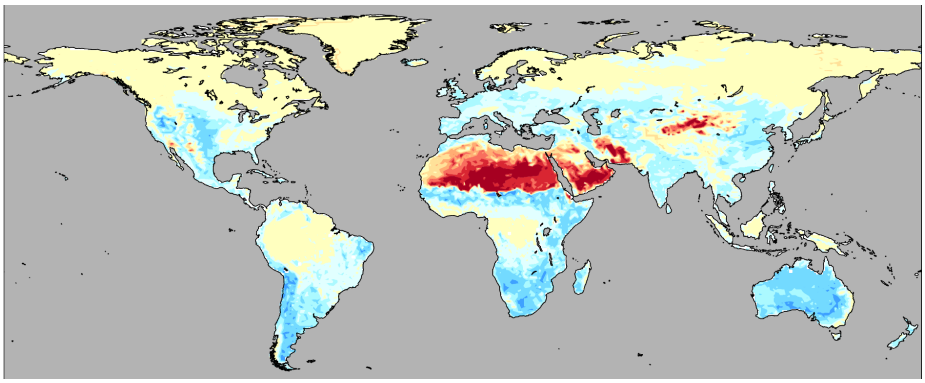

(b) V polarisation

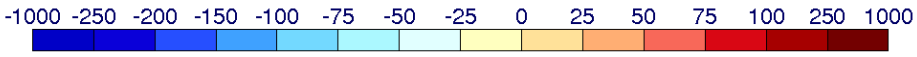

Figure 16: Averaged first component of the SMOS Jacobian (see section 2.3) for March, April and May 2011. Top plot is for XX polarisation and bottom plot for YY polarisation.

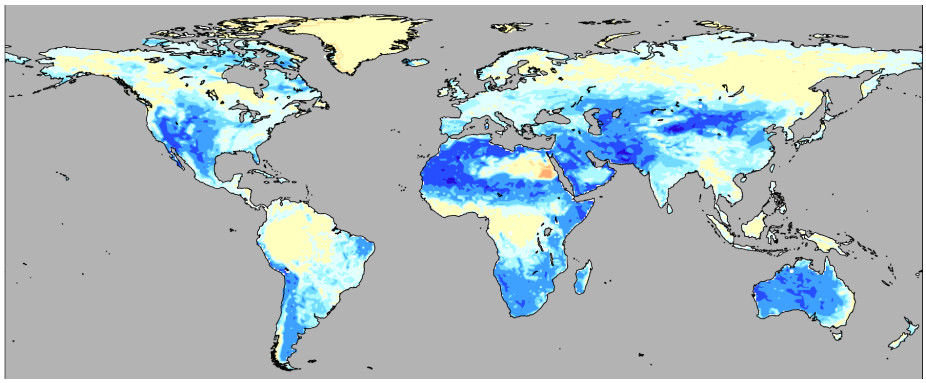

(a) H polarisation

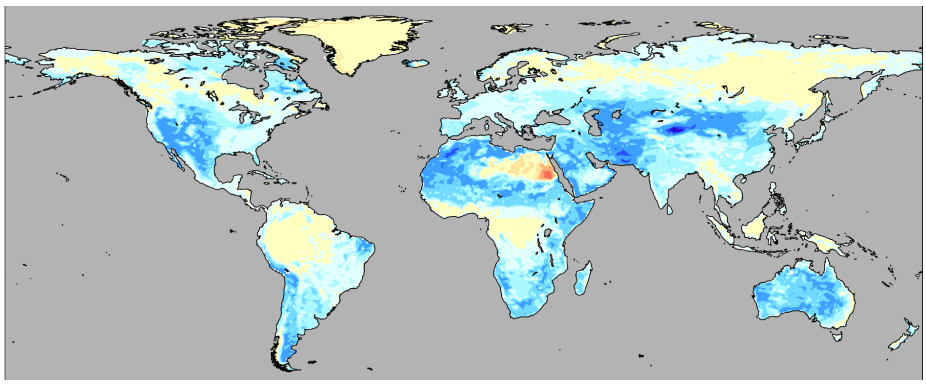

(b) V polarisation

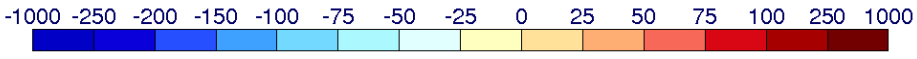

Figure 17: As Fig. 16, but average is over September, October and November 2010.

5 References

References

[1] G. Balsamo, P. Viterbo, A. Beljaars, B. van den Hurk, M. Hirschi, A.K. Betts, and K. Scipal. A revised hydrology for the ECMWF model: Verification from field site to terrestrial water storage and impact in the integrated forecast system. *Journal of Hydrometeorology*, 10:623–643, 2009. doi: 10.1175/2008JHM1068.1.

[2] S. Boussetta, G. Balsamo, A. Beljaars, and J. Jarlan. Impact of a satellite-derived leaf area index monthly climatology in a global numerical weather prediction model. *International Journal of Remote Sensing*, 2013.

[3] P. de Rosnay, M. Drusch, A. Boone, G. Balsamo, B. Decharme, P. Harris, Y. Kerr, T. Pellarin, J. Polcher, and J.-P. Wigneron. AMMA Land Surface Model Intercomparison Experiment coupled to the Community Microwave Emission Model: ALMIP-MEM. *J. Geophys. Res.*, 114, 2009. D05108, doi:10.1029/2008JD010724.

[4] P. de Rosnay, M. Drusch, and J.Muñoz-Sabater. Milestone 1 Technical Note Part I: SMOS global surface emission model. Technical report, European Centre for Medium-Range Weather Forecast, Reading, United Kingdom, november 2009.

[5] P. de Rosnay et al. SMOS Report on bias correction. Technical report, European Centre for Medium-Range Weather Forecasts, Reading, United Kingdom, 2014.

[6] M. Drusch, T. Holmes, P. de Rosnay, and G. Balsamo. Comparing ERA-40 based L-band brightness temperatures with Skylab observations: A calibration / validation study using the Community Microwave Emission Model. *J. Hydrometeor.*, 10:213–226, 2009. doi: 10.1175/2008JHM964.1.

[7] J. Muñoz-Sabater et al. SMOS Data Assimilation Impact Report. Technical report, European Centre for Medium-Range Weather Forecasts, Reading, United Kingdom, January 2014.

[8] R. D. Koster, P. A. Dirmeyer, Z. Guo, G. Bonan, E. Chan, P. Cox, C. T. Gordon, S. Kanae, E. Kowalczyk, D. Lawrence, P. Liu, C. Lu, S. Malyshev, B. McAvaney, K. Mitchell, D. Mocko, T. Oki, K. Oleson, A. Pitman, Y. C. Sud, C. M. Taylor, D. Verseghy, R. Vasic, Y. Xue, and T. Yamada. Regions of strong coupling between soil moisture and precipitation. *Science*, 305(5687):1138–1140, 2004.

[9] J. Muñoz-Sabater, M. Dahoui, P. de Rosnay, and L. Isaksen. SMOS Monitoring Report; Part II. Technical report, European Centre for Medium-Range Weather Forecasts, Reading, United Kingdom, December 2011.

[10] J. Muñoz-Sabater, M. Dahoui, P. de Rosnay, and L. Isaksen. SMOS Level 3 Root Zone Soil Moisture Report. Technical report, European Centre for Medium-Range Weather Forecasts, Reading, United Kingdom, January 2014.

[11] J. Muñoz-Sabater and P. de Rosnay. Tech note- Part III- WP1300: SMOS Report on Noise Filtering. Technical report, European Centre for Medium-Range Weather Forecasts, Reading, United Kingdom, November 2011.

[12] J. Muñoz-Sabater, P. de Rosnay, and M. Dahoui. SMOS Continuous Monitoring Reports; Part I. Technical report, European Centre for Medium-Range Weather Forecasts, Reading, United Kingdom, February 2011.

[13] J. Muñoz-Sabater, P. de Rosnay, A. Fouilloux, M. Dahoui, L. Isaksen, C. Albergel, I. Mallas, and T. Wilhelmsson. Phase I, Final Report. Technical report, European Centre for Medium-Range Weather Forecasts, Reading, United Kingdom, January 2013.

[14] J. Muñoz-Sabater, P. de Rosnay, and G.Balsamo. Sensitivity of L-band NWP forward modelling to soil roughness. *Int. J. Remote Sens.*, 32(19):5607–5620, 2011. iFirst 2011., doi: 10.1080/01431161.2010.507260.

[15] T. Pellarin, J.-P. Wigneron, J.-C. Calvet, and P. Waldteufel. Global soil moisture retrieval from a synthetic l-band brightness temperature data set. *Journal of Geophysical Research*, 108(4364, doi:10.1029/2002JD003086), 2003.

[16] R.D.Koster and Coauthors. The Global Land-Atmosphere Coupling Experiment. Part I: Overview. *J. Hydrometeor.*, 7:590–610, 2006.

[17] R. Salgado. Global soil maps of sand and clay fractions and of the soil depth for MESONH simulation based on FAO/UNESCO soil maps. Technical report, CNRM/Météo France, 1999. Tech. Note, **59**.

[18] J. R. Wang and T. Schmugge. An empirical model for the complex dielectric permittivity of soils as a function of water content. *IEEE Transactions on Geoscience and Remote Sensing*, 18:288–295, 1980.

[19] J.-P. Wigneron, Y. Kerr, P. Waldteufel, K. Saleh, M.-J. Escorihuela, P. Richaume, P. Ferrazzoli, P. de Rosnay, R. Gurneye, J.-C. Calvet, J.P. Grant, M. Guglielmetti, B. Hornbuckle, C. Mtzler, T. Pellarin, and M. Schwank. L-band microwave emission of the biosphere (L-MEB) model: Description and calibration against experimental data sets over crop fields. *Remote Sensing of Environment*, 107(4):639–655, 2007.

[20] J. P. Wigneron, L. Laguerre, and Y. Kerr. A simple parameterization of the L-band microwave emission from rough agricultural soils. *IEEE Transactions on Geoscience and Remote Sensing*, 39:1697–1707, 2001.